DESIGN AND PERFORMANCE OF A STIFF WAVE BARRIER IN THE SOIL

CONCEPTION ET PERFORMANCE D'UNE BARRIERE D'ONDES RAIDE DANS LE SOL

Pieter COULIER[1], Stijn FRANÇOIS[1], Vicente CUÉLLAR[2], Geert DEGRANDE[1], Geert LOMBAERT[1]

[1]*KU Leuven, Department of Civil Engineering, Kasteelpark Arenberg 40, 3001 Leuven, Belgium*
[2]*CEDEX, Laboratoria de Geotecnica, Alfonso XII 3, 28014 Madrid, Spain*

ABSTRACT – This paper investigates the effectiveness of a stiff wave barrier in the soil as an efficient measure for the mitigation of railway induced vibrations. Numerical calculations demonstrate that such a barrier can be very effective, provided that the stiffness contrast between the barrier and the surrounding soil is sufficiently large. Findings from the numerical studies are verified by means of a field test in Spain, where a continuous barrier has been created close to an existing railway track using overlapping jet grout columns. Measurements of train passages before and after installation of the barrier are compared in order to assess the barrier's vibration reduction efficiency. It is shown that the jet grouting wall is very effective: immediately behind the wall, insertion loss values of about 5 dB are already obtained from 8 Hz on, with a peak of about 12 dB at 25 Hz. The barrier's ability to solve low frequency vibration problems is a unique feature compared to most other vibration mitigation measures for existing railway lines.

RÉSUMÉ – Cet article étudie l'efficacité d'une barrière d'ondes raide dans le sol comme une mesure pour l'atténuation des vibrations induites par le trafic ferroviaire. Des simulations numériques montrent qu'une telle barrière peut être très efficace, à condition que le contraste de la raideur entre la barrière et le sol soit suffisamment grand. Les résultats des études numériques sont vérifiés au moyen d'un test sur site en Espagne, où une barrière raide a été créée le long d'une voie ferrée existante. Des mesures de passages de trains avant et après la création de la barrière sont comparés afin d'évaluer l'efficacité de réduire des vibrations. Il est démontré que la barrière est très efficace: une réduction de l'ordre de 5 dB est déjà obtenue à partir de 8 Hz, avec un maximum de 12 dB observé auprès de 25 Hz. Cette capacité de réduire des vibrations à basses fréquences est unique par rapport à la plupart des autres mesures d'atténuation des vibrations pour des lignes ferroviaires existantes.

1. Introduction

During the past decades, a lot of research has been performed to develop efficient and cost–effective vibration countermeasures for reducing the levels of railway induced building vibration (Jones, 1994; Kaynia et al., 2000). Measures can either be taken at the source (Lombaert et al., 2006), on the propagation path between source and receiver (Karlström and Boström, 2007), or at the receiver (Talbot and Hunt, 2003). An advantage of interventions on the propagation path is that no modifications of the track are required, while multiple buildings can be shielded simultaneously from vibration. Furthermore, this

type of measures can relatively easily be implemented in existing situations. Typical examples are vibration isolation screens (Woods, 1968), buried wall barriers (Andersen and Nielsen, 2005), and wave impeding blocks (Sheng et al., 2005).

Within the frame of the EU FP7 project RIVAS (RIVAS, 2011), several mitigation measures on the propagation path between source and receiver have been investigated in detail. This paper focuses on so–called stiff wave barriers (i.e. barriers consisting of material that is stiffer than the surrounding soil) as efficient vibration countermeasures. Recent numerical simulations have demonstrated that a stiff barrier can hinder the transmission of waves in the soil and act as an effective wave impeding barrier (Coulier et al., 2013a). These simulations have furthermore allowed establishing the circumstances in which a stiff barrier is efficient, highlighting how the performance depends on site specific characteristics such as the dynamic soil properties. It is crucial, however, to verify the predicted mitigation performance through experiments. A full-scale field test has therefore been performed in El Realengo (Spain), which is the topic of this paper.

The text is organized as follows. Section 2 recapitulates the main findings from recent numerical studies and indicates how a stiff wave barrier behaves. The field test in El Realengo (Spain) is subsequently introduced in section 3. The experimental results are discussed and compared with results from numerical simulations. This allows for a physical interpretation of the experimental results and also reveals to what extent numerical simulations can be used for designing these mitigation measures. Final conclusions are summarized in section 4.

2. Numerical simulations: physical mechanism

The vibration reduction effectiveness of a stiff wave barrier has been analyzed in detail in (Coulier et al., 2013a) using a coupled finite element – boundary element (FE–BE) methodology (François et al., 2010). The physical mechanism is briefly discussed in the following for a (hypothetical) case study of a barrier in a homogeneous halfspace.

The halfspace is characterized by a shear wave velocity C_s = 200 m/s, a dilatational wave velocity C_p = 400 m/s, a density ρ = 2000 kg/m^3, and material damping ratios $\beta_s = \beta_p$ = 0.025 in both deviatoric and volumetric deformation. The stiff wave barrier is assumed to be of infinite length and has a width w = 2 m and a depth h = 2 m. This barrier has a shear wave velocity C_s = 550 m/s and a dilatational wave velocity C_p = 950 m/s; the same density and material damping ratios as in the halfspace are used. To facilitate physical interpretation, an incident wavefield is generated by the application of a unit vertical harmonic point load at the surface of the halfspace; the presence of the railway track is thus neglected.

The wave impeding effect of the stiff wave barrier is illustrated in figure 1. Figures 1a and 1b show the vertical wavefield in the soil at a frequency of 45 Hz in the reference case (i.e. without barrier) and in case the barrier is included, respectively. A cylindrical wavefield with a Rayleigh wavelength $\lambda_R = C_R / f$ = 4.1 m can clearly be observed in the reference case (where C_R is the Rayleigh wave velocity in the soil). The wavefield is considerably perturbed, however, with the stiff wave barrier embedded in the soil. The vibration reduction efficiency of the barrier is quantified through the vertical insertion loss:

$$\mathrm{IL}_z\left(\mathbf{x}, f\right) = 20\log_{10}\frac{\left|u_z^{\mathrm{ref}}\left(\mathbf{x}, f\right)\right|}{\left|u_z\left(\mathbf{x}, f\right)\right|} \quad [\mathrm{dB}] \tag{1}$$

where $u_z^{\mathrm{ref}}\left(\mathbf{x}, f\right)$ and $u_z\left(\mathbf{x}, f\right)$ represent the vertical free-field displacement in the reference case (without barrier) and in the case with the barrier, respectively. Positive

values of the insertion loss indicate a reduction of the vertical free-field vibration. The insertion loss $\mathrm{IL}_z(\mathrm{x}, f)$ is shown in figure 1c. A delimited area where significant reduction of vibration levels is achieved is observed. The insertion loss reaches values of 10 dB and more in this region. The reduction is not only obtained at the surface of the halfspace, but also at depth, although some localized areas can be identified with increased vibration levels with respect to the reference case. Furthermore, lines of constructive and destructive interference between direct and reflected Rayleigh waves can be observed at the opposite side of the barrier.

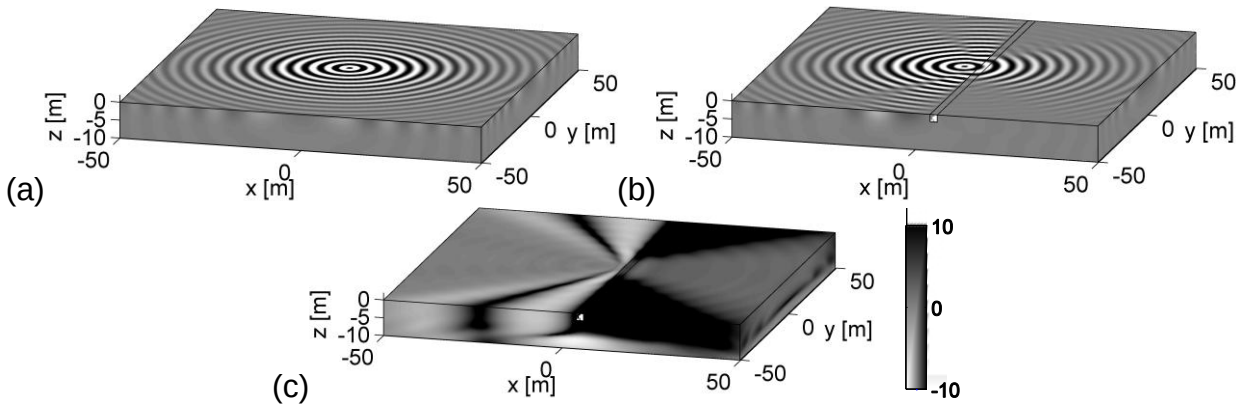

Figure 1. Real part of the vertical displacement in the soil due to a unit harmonic vertical excitation at the origin of the coordinate system at 45 Hz (a) on a homogeneous halfspace and (b) when a stiff wave barrier is included. The vertical insertion loss is shown in (c).

As discussed in (Coulier et al., 2013), the peculiar pattern observed in figures 1b and 1c is due to the interaction between Rayleigh waves in the soil and bending waves in the stiff wave barrier. The propagation of plane waves in the soil with a trace wavelength smaller than the barrier's bending wavelength is impeded due to the latter's bending stiffness. This only occurs above a critical frequency at which the Rayleigh wavelength in the soil matches the free bending wavelength in the barrier. A critical angle delimiting an area where vibration levels are reduced can be defined as well, determined by the ratio of the Rayleigh wavelength in the soil and the free bending wavelength in the barrier. This angle can clearly be distinguished in figure 1c. Expressions for the critical frequency and angle are provided in (Coulier et al., 2013). Both quantities depend on the stiffness contrast between the soil and the barrier; stiff barriers are the most efficient in soft soils. Numerical simulations furthermore indicate that a stiff barrier behaves in a similar way if embedded in layered halfspace (instead of a homogeneous halfspace).

The vibration reduction efficiency of a stiff barrier has also been investigated during the passage of a train. In that case, multiple dynamic axle loads (e.g. originating from the track unevenness) contribute to the free field vibration. Due to the existence of a critical angle, the presence of a stiff barrier results in a larger reduction of vibration levels just behind the barrier than further away.

3. Experimental validation: jet grouting wall

3.1. Description of the test site and design of the stiff barrier

In order to verify the findings from the numerical studies, a field test has been designed within the frame of RIVAS. A suitable site has been identified in El Realengo (south–east of Spain) along the conventional railway line between Murcia and Alicante. Previous

geotechnical studies indicated the presence of soft soil layers at this site, which is a situation in which a stiff barrier is expected to be very effective. At the site, a test section as well as a reference section have been identified. The jet grouting wall is implemented along the test section; the aim of the reference section is to control changing track, train, and soil conditions over time.

Geophysical tests have been performed in April 2012 for the determination of the dynamic soil characteristics (Coulier et al., 2013b). This includes Spectral Analysis of Surface Waves (SASW) tests, seismic piezocone down–hole tests (SCPTU), and seismic refraction tests. These tests have allowed for the identification of a simplified horizontally layered soil model, as summarized in table 1 (layer thickness h, shear wave velocity C_s, dilatational wave velocity C_p, material damping ratios β_s and β_p in both deviatoric and volumetric deformation, density ρ). The soil density values given in the table are those determined from undisturbed samples retrieved from the boreholes drilled in previous geotechnical studies. The identified soil profile confirms the presence of a soft layer of silty clay with a thickness of ±10 m (layers 2 and 3) that overlies hard alluvial soil.

Table 1. Dynamic soil characteristics at the site in El Realengo.

Layer	h [m]	C_s [m/s]	C_p [m/s]	β_s [-]	β_p [-]	ρ [kg/m^3]
1	0.30	270	560	0.123	0.123	1800
2	1.20	150	470	0.112	0.112	1750
3	8.50	150	1560	0.014	0.014	1750
4	10.00	475	1560	0.010	0.010	1900
5	∞	550	2030	0.010	0.010	1900

The stiff wave barrier is designed as a jet grouting wall composed of overlapping grout columns (figure 2). Based on the preliminary design (Coulier et al., 2013b), a jet grouting wall with a depth of 7.5 m, a width of 1 m, and a length of 55 m has been constructed adjacent to the railway track. The diameter of the individual columns is 1.5 m. For safety reasons, the jet grouting wall has been constructed at a distance of 16.2 m from the track.

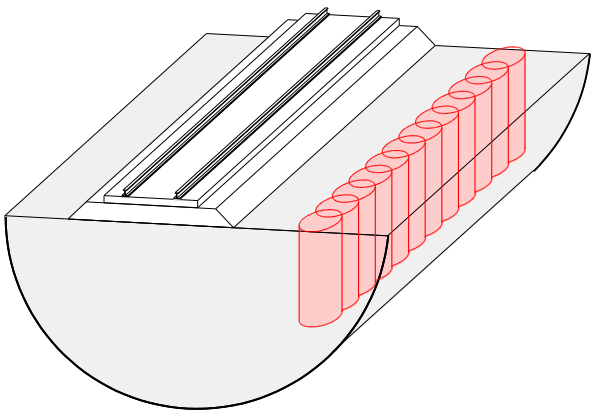

(a)

(b)

Figure 2. (a) Sketch of the stiff wave barrier consisting of overlapping jet grout columns and (b) the stiff wave barrier after construction at the site of El Realengo.

During installation of the jet grouting wall, multiple test samples have been taken out to verify its strength and stiffness. Laboratory tests (unconfined compression tests, non dispersive P-S sonic tests, dispersive bender element tests) have been performed on these samples; the best estimate of the dynamic characteristics (two months after

construction) is given in table 2. The lower part of the barrier is saturated, resulting in a variation of the dilatational wave velocity C_p with depth.

Table 2. Dynamic characteristics of the jet grouting wall. Estimated values are indicated by a star.

Layer	h [m]	C_s [m/s]	C_p [m/s]	β_s [-]	β_p [-]	ρ [kg/m^3]
1	1.50	600	1150	0.03*	0.03*	1400
2	6.00	600	1650	0.03*	0.03*	1400

The track at the test site is a classical ballasted track with bi–block reinforced concrete sleepers supporting RN 45 rails with Spanish gauge. The ballast layer with a height of 0.50 m is supported by an embankment 0.50 m high. The reader is referred to (Verbraken et al., 2013) for a detailed description of the test site.

3.2. Experimental evaluation of the mitigation performance

Extensive measurement campaigns have been carried out before (October 2013) and after (December 2013) construction of the jet grouting wall. Since some time was needed for the grout to harden out, vibration measurements after the construction of the jet grouting wall were performed one month after construction. Transfer functions as well as train pass–bys have been measured, both at the test section and at the reference section.

This paper only reports on the experimental results obtained during train pass–bys. A total of 28 and 30 train passages have been recorded before and after construction, respectively, of three different train types: S592 commuter trains, S599 medium distance trains, and long distance Talgo VI trains. In the following, results obtained during the passage of S592 trains are discussed, as similar trends are revealed for the other train types. The S592 commuter train is a short train consisting of three carriages. Each carriage has two bogies, one in the front and one in the back. Each bogie is supported by two axles. The train has a total length of 65 m between the first and last axle. Each axle has an estimated unsprung mass of 2000 kg.

As only a single track is present at the site, both train passages from Murcia to Alicante and vice versa are recorded. The train velocities are estimated based on strain measurements on the rails at the reference and test site. The train speed varies between 112 km/h and 122 km/h for the S592 commuter trains (with an average speed of 117 km/h). Free field vertical vibration velocities were measured by means of geophones along a line perpendicular to the track, at 10 m, 14 m, 18 m, and 32 m from the outer rail, both at the reference and test site. The receiver locations at 18 m and 32 m are situated behind the jet grouting wall.

The vibration velocity level $L_v(f)$ during a train passage is defined as the one–third octave band spectrum of the stationary part of the vibration velocity. The stationary part of the measured response during a train passage can be selected using the German DIN standard (DIN, 1995). Figure 3 shows the measured vibration velocity levels $L_v(f)$ during the passages of all S592 commuter trains before and after construction of the jet grouting wall, where different train velocities are indicated with a different shade (a lighter shade indicates a higher velocity). It is observed that the vibration velocity level $L_v(f)$ decreases with increasing distance from the track; especially the high frequency components are attenuated due to material damping in the soil. Before construction of the jet grouting wall, a clear peak of $L_v(f)$ near 25–30 Hz can be distinguished at 10 m, 14 m, and 18 m from the track. This peak is more pronounced at the test site than at the reference site.

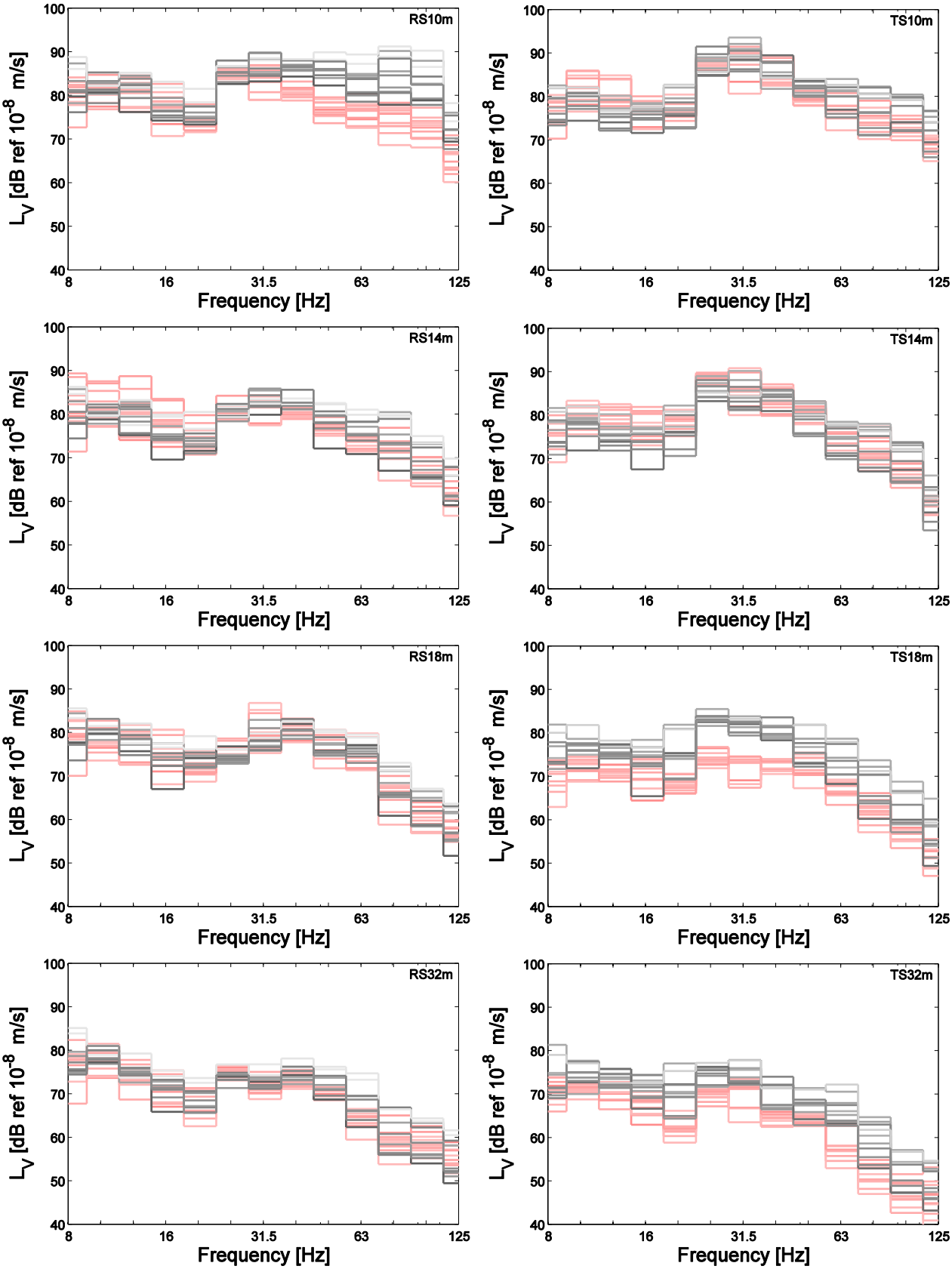

Figure 3. Measured vibration velocity levels $L_V(f)$ in one–third octave bands at the reference (left) and the test site (right) during the passage of S592 commuter trains before (grey) and after (red) construction of the jet grouting wall. The average train speed is 117 km/h. The jet grouting wall is situated at 16.2 m from the track center.

The vibration reduction efficiency of the jet grouting wall is quantified through the vertical insertion loss $IL_z(f)$ (Stiebel, 2011):

$$\mathrm{IL}_z\left(f\right)=\left(L_\mathrm{v}^{\mathrm{test,before}}\left(f\right)-L_\mathrm{v}^{\mathrm{test,after}}\left(f\right)\right)-\left(L_\mathrm{v}^{\mathrm{ref,before}}\left(f\right)-L_\mathrm{v}^{\mathrm{ref,after}}\left(f\right)\right) \quad (2)$$

The first bracketed term in equation (2) characterizes the reduction of vibration levels at the test site (comparing $L_v(f)$ before and after construction of the jet grouting wall), while the second term is a correction for possible variations in time (based on measurements at the reference site). The resulting insertion loss values obtained from the passage of S592 commuter trains are shown in figure 4. Immediately behind the wall (at 18 m), insertion loss values of about 5 dB are already obtained from 8 Hz on, with a peak of about 12 dB at 25 Hz, which is also the frequency range where the highest vibration levels are found during train pass–bys. This corresponds to a reduction by a factor of four. As expected, the insertion loss values decrease further away from the jet grouting wall (at 32 m), although it still reaches almost 8 dB at 25 Hz (a reduction by a factor of 2.5). A slight amplification of vibration levels is observed at the opposite side of the barrier (at 10 m and 14 m).

The results in figures 3 and 4 indicate that the jet grouting wall is able to reduce the vibration levels during train passages from relatively low frequencies, which is a unique feature compared to most other vibration mitigation measures described in the literature.

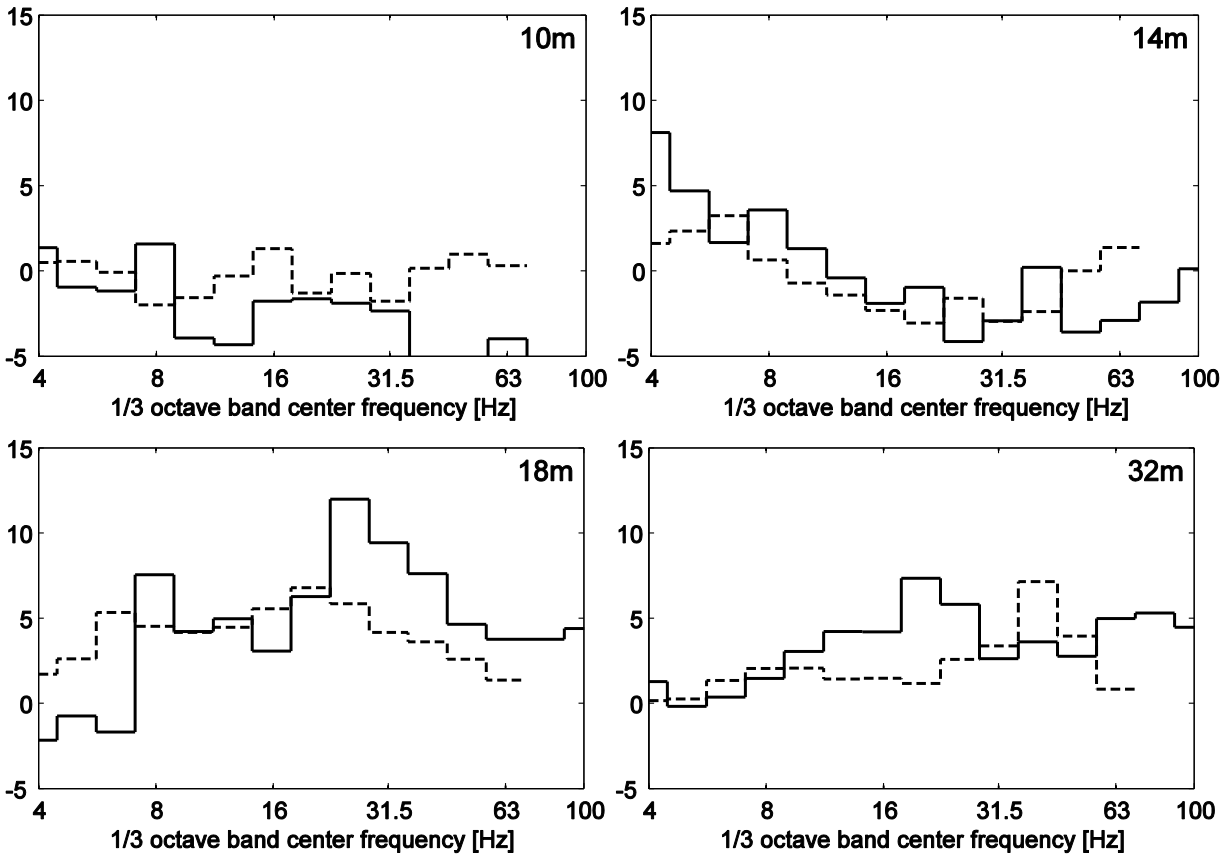

Figure 4. Measured (black line) and calculated (dashed line) vertical insertion loss values $IL_z(f)$ in one–third octave bands for the passage of S592 commuter trains at an average speed of 117 km/h. The jet grouting wall is situated at 16.2 m from the track center.

3.3 Comparison with simulations

The experimental results are compared to numerical simulations that have been performed by means of a 2.5D coupled FE–BE methodology (Coulier et al., 2013a; François et al., 2010). The dynamic axle loads depend on the unevenness experienced by the wheels at the wheel–rail interface. No information is available about the unevenness at the site in El Realengo, however; an unevenness profile corresponding to a poor track quality has been employed in the numerical simulations, using an FRA track class 1 defined by the Federal Railroad Administration (FRA). Consequently, it is impossible to provide a fair comparison of measurements and predictions in terms of the vibration velocity levels $L_v(f)$. Therefore, a comparison of the insertion loss $IL_z(f)$ is presented. Due to computational limitations, the simulations are limited to 72 Hz.

Superimposed on figure 4 are predicted insertion loss values $IL_z(f)$ for the passage of S592 trains. A reasonable qualitative agreement between the measurements and predictions is observed, as the same trends are revealed. A slight amplification is predicted in front of the barrier, and a peak in the insertion loss near 25 Hz is predicted at 18 m. The predicted insertion loss also decreases at larger distances from the barrier. The observed deviations between measurements and predictions of ±5 dB are of the same order of magnitude as the common uncertainty in the prediction of railway induced vibrations (Hunt and Hussein, 2007). This indicates that state–of–the–art numerical prediction models can be used for the reliable design of stiff wave barriers.

The simulations tend to underestimate the measured insertion loss values behind the wall. A possible explanation for the observed discrepancy could be the fact that the soil surrounding the jet grouting wall has been stiffened during the installation of the jet grout columns. As a result, it is likely that a wave barrier with a larger width than assumed in the calculations has been created in reality, which results in a better performance of the barrier. The discrepancies between the measurements and predictions could also be caused by simplifications introduced in the numerical model, such as the assumption that the jet grouting wall is of infinite length and the fact that a simplified vehicle model is used (i.e. only the unsprung axle masses are accounted for, which is inaccurate at low frequencies).

4. Conclusion

This paper describes the design and experimental testing of a stiff wave barrier at a site in El Realengo. A jet grouting wall with a width of 1 m, a depth of 7.5 m, and a length of 55 m has been installed at this site, and free field vibrations during multiple train pass–bys have been measured before and after installation. The experimental results show that the jet grouting wall is very effective. Immediately behind the wall, insertion loss values of about 5 dB are already obtained from 8 Hz on, with a peak of about 12 dB at 25 Hz, which is also the frequency range where the highest vibration levels are found during a train pass–by. As predicted, the insertion loss values decrease further away from the jet grouting wall. The measured insertion loss values are consistently higher than the predicted values, which is believed to be caused by the fact that the soil surrounding the wall has been stiffened by the installation of the jet grout columns.

The field test shows that a stiff wave barrier is able to solve low frequency vibration problems, provided that is properly designed and sufficiently stiff compared to the soil in which it is installed. This ability to reduce low frequency vibration is a unique feature, distinguishing this vibration mitigation measure from most other measures reported in the literature. The observed differences between the experimental and numerical results are reasonable in view of the significant uncertainty in the prediction of railway induced

vibrations, indicating that state–of–the–art numerical prediction models can be used for design of stiff wave barriers.

Acknowledgments

The results presented in this paper have been obtained within the frame of the EU FP7 project RIVAS (Railway Induced Vibration Abatement Solutions) under grant agreement No. 265754. The first and second author are fellows of the Research Foundation Flanders (FWO). The financial support is gratefully acknowledged.

References

http://www.rivas-project.eu (2011).

Andersen L. and Nielsen S.R.K. (2005). Reduction of ground vibration by means of barriers or soil improvement along a railway track. *Soil Dynamics and Earthquake Engineering*, 25:701–716.

Coulier P., François S., Degrande G., and Lombaert G. (2013a). Subgrade stiffening next to the track as a wave impeding barrier for railway induced vibrations. *Soil Dynamics and Earthquake Engineering*, 48:119–131.

Coulier P., Degrande G., Dijckmans A., Lombaert G., Cuéllar V., Yuste M., Müller R., Vucotic G., Keil J., Auersch K., Knothe E., Rücker W., Said S., Jiang J., Thompson D.J., and Toward M.G.R. (2013b). Design of the mitigation measures at the test sites. RIVAS project SCP0-GA-2010-265754, Deliverable D4.3, Report to the EC.

Deutsches Institut für Normung (1995). *DIN 45672 Teil 2: Schwingungsmessungen in der Umgebung von Schienenverkehrswegen: Auswerteverfahren*.

François S., Schevenels M., Lombaert G., Galvín P., and Degrande G. (2010). A 2.5D coupled FE-BE methodology for the dynamic interaction between longitudinally invariant structures and a layered halfspace. *Computer Methods in Applied Mechanics and Engineering*, 199(23-24):1536–1548.

Hunt H.E.M. and Hussein M.F.M. (2007). Vibration from railways: can we achieve better than +/-10 dB prediction accuracy? In *14th International Congress on Sound and Vibration*, Cairns, Australia.

Jones C.J.C. (1994). Use of numerical-models to determine the effectiveness of anti-vibration systems for railways. *Proceedings of the Institution of Civil Engineers-Transport*, 105(1):43–51.

Karlström A. and Boström A. (2007). Efficiency of trenches along railways for trains moving at sub- or supersonic speeds. *Soil Dynamics and Earthquake Engineering*, 27:625–641.

Kaynia A.M., Madshus C., and Zackrisson P. (2000). Ground vibration from high speed trains: prediction and countermeasure. *Journal of Geotechnical and Geoenvironmental Engineering, Proceedings of the ASCE*, 126(6):531–537.

Lombaert G., Degrande G., Vanhauwere B., Vandeborght B., and François S. (2006). The control of ground borne vibrations from railway traffic by means of continuous floating slabs. *Journal of Sound and Vibration*, 297(3-5):946–961.

Sheng X., Jones C.J.C., and Thompson D.J. (2005). Modelling ground vibrations from railways using wavenumber finite- and boundary-element methods. *Proceedings of the Royal Society A - Mathematical, Physical and Engineering Sciences*, 461:2043–2070.

Stiebel D. (2011). Protocol for free field measurements of mitigation effects in the project RIVAS for WP 2, 3, 4, 5. RIVAS project SCP0-GA-2010-265754, Deliverable D1.2, Report to the EC.

Talbot J.P. and Hunt H.E.M. (2003). A generic model for evaluating the performance of base-isolated buildings. *Journal of Low Frequency Noise, Vibration and Active Control*, 22(3):149–160.

Verbraken H., Degrande G., Lombaert G., Stallaert B., and Cuéllar V. (2013). Benchmark tests for soil properties, including recommendations for standards and guidelines. RIVAS project SCP0-GA-2010-265754, Deliverable D1.11, Report to the EC.

Woods R.D. (1968). Screening of surface waves in soils. *Journal of the Soil Mechanics and Foundation Division, Proceedings of the ASCE*, 94(SM4):951–979.